Cracking Behavior of CFRP Laminate-Strengthened RC Beams with Pre- and Post-Mechanical and Environmental Damage

Dawei Zhang [1)], ShijunShen[1)], Yuxi Zhao*[1)], Weiliang Jin[1)], Tamon Ueda[2)]

1) Institute of Structural Engineering, Zhejiang University, Hangzhou, China, 310058

2) Lab of Engineering for Maintenance System, Hokkaido University, Sapporo, Japan, 060-8628

Abstract: The main objectives of this study are to investigate the effects of three types of pre- and post-damages on the cracking behaviors of carbon fiber-reinforced polymer (CFRP)-strengthened reinforced concrete RC beams and to develop a rational methodology for predicting the average stabilized crack spacing. The pre-damage is induced by either sustained loading only or by the combination of sustained loading and corrosion. The pre-damage involved a sustained loading with an anchor tightening system, an electrochemical process to accelerate the migration of chlorides from an external electrolyte into the tested beams, and a wetting–drying cycle process with a controlled current to accelerate the corrosion of the reinforcing steel bars in the tested beams. The post-damage was induced by wetting-drying cycles. A loading test was conducted to determine the cracking behaviors of stabilized flexural cracks in the CFRP-strengthened beams with or without damage. The crack patterns, crack spacings and test beam widths were recorded and compared, and the related mechanism was discussed. It was found that after CFRP strengthening, the effect of pre- or post-damage on the crack spacing and width is not as distinct as in the un-strengthened cases. The sustained loading pre-damaged beam showed insignificant differences in crack spacing and width compared to beams without pre-damage. Subsequently, a model capable of evaluating the

crack behaviors of CFRP-strengthened beams with or without damage was developed. The analytical approach is based on equilibrium and compatibility equations to elucidate the average stresses of concrete and the CFRP laminate of a CFRP-strengthened beam element.

Keywords: crack spacing; CFRP; strengthening; interface; bond; corrosion

Introduction

The effectiveness of fiber-reinforced polymer (FRP) systems in increasing the structural capacities of RC members under external loading has been reported in numerous studies (Hollaway and Leeming 2000; Oehlers 2001). In field conditions, reinforced concrete (RC) structures are generally exposed to a wide variety of combined loading and environmental actions. These actions can occur throughout the entire service life of RC members, including the pre- and post-strengthening stages. The prediction of service life with strengthening will only become realistic when pre- and post-damage caused by the combination of loads and environmental actions are taken into consideration.

Flexural cracks in CFRP-strengthened RC structures may be expected because of the relatively low tensile strength of concrete. Cracking in strengthened RC structures has a major influence on structural performance, including tensile, bending and shear stiffnesses; energy absorption capacity; ductility; and corrosion resistance of the reinforcement. Moreover, the average crack spacing of

strengthened beams plays an important role in the transfer of shear stress along the CFRP laminate-substrate interface with concrete and in the normal stress generated in the concrete substrate in the case when premature debonding failure, such as CFRP peeling or concrete cover separation, is investigated (Zhang et al. 2011; Wang and Ling 1998;Raoof and Hassanen 2000). Therefore, it is necessary to predict the cracking behavior of CFRP-strengthened RC beams.

Tensile cracking in strengthened concrete members is affected by various factors, such as the types of reinforcement, concrete cover thickness, effective cross-sectional area of concrete, diameter of reinforcement, ratio of reinforcement, number of layers of reinforcement, surface geometry of reinforcement, quality of concrete, and magnitude of pre-stress. Corrosion of the reinforcement is one of the major causes of deterioration in reinforced concrete structures. Moreover, the chloride penetration with load combination is among the most frequent origins for early and excessive damage of RC structures situated in marine environments or exposed to de-icing salt during the winter period. Consequently, the primary mechanism for the bond strength between deformed bars and concrete is deteriorated. Carbon fiber sheets are considered to be a highly durable material with very good resistance against harsh environments (Saadatmanesh et al. 2010; Sciolti et al. 2010). The harmful effects of water or corrosive solutions on the properties of the epoxy resins used for CFRP bonding are reported to be plasticization, hydrolysis, cracking and crazing, which can directly affect the mechanical properties of the resin and its bonding to the concrete substrate (Lau and Büyüköztürk 2010; Tuakta and Büyüköztürk 2011; Mays and Hutchinson 1992). The change in the

bonding properties of the CFRP-concrete interface due to moisture may affect the cracking behavior of CFRP-strengthened RC members. Although many studies have been conducted by different researchers regarding the effects of either pre- or post-damages on the structural performances of CFRP-strengthened RC members (Badawi and Soudki 2010; Bonacci and Maalej 2000; Debaiky et al. 2002; EI Maaddawy and Soudki 2005; Masoud et al. 2001; Masoud and Soudki 2006; Nossoni and Harichandran 2009; Wang et al. 2004; Wootton et al. 2003), thorough comparisons of CFRP-strengthened beams of pre- and post-damage have not been conducted: 1. Pre-damage with sustained loading, 2. pre-damage with combined sustained loading and bar corrosion, and 3. post-damage with wetting-drying cycles. Although some models have been developed for the average crack spacing in CFRP-strengthened RC members (Raoof and Hassanen 2000; Ceroni and Pecce 2009; Zhang et al. 2012), a reliable model for the cases with pre- or post-damage still needs to be developed and examined.

The main objectives of this study are to investigate and compare the effects of the above three types of pre- and post-damages on the cracking behavior of CFRP-strengthened RC beams and to develop a rational methodology for predicting the average stabilized crack spacing. The pre-damage is induced by either sustained loading only or by the combination of sustained loading and corrosion. The pre-damage involved a sustained loading with an anchortightening system, an electrochemical process to accelerate the migration of chlorides from an external electrolyte into the tested beams,

and a wetting–drying cycle process with a controlled current to accelerate the corrosion of the reinforcing steel bars in the tested beams. The post-damage was induced by wetting-drying cycles after CFRP strengthening. A loading test was conducted to determine the cracking behaviors of the beams with or without damage before and after strengthening. Subsequently, a model capable of evaluating the crack behaviors of CFRP-strengthened beams with or without damage was developed. The analytical approach is based on equilibrium and compatibility equations to elucidate the average stresses of concrete and the CFRP laminate of a CFRP-strengthened beam element.

Test Program

Table 1 summarizes the experimental program. In total, 12 beams were tested. The acronym designation adopted for the specimens was as follows: “C” represents corrosion pre-damage, and “L” means sustained pre-loading damage; “S” stands for CFRP strengthening; and the last number corresponds to the number of wetting-dying cycles after strengthening. For example, specimen “L-C-S-40” is the CFRP-strengthened beam with combined pre-loading and corrosion damage before strengthening and 40 wetting-drying cycles after strengthening.

Fig. 1 presents the geometry and reinforcement details of the tested specimens. The specimens had a cross section of 120 x 200 mm. The total length of the specimen was 2,000 mm, with a clear span

of 1,800 mm. For tension reinforcement, the beams were reinforced with two B12 mm (HRB 335) deformed steel bars that were hooked at the ends of the beams to avoid any premature bond failure. Two ϕ 8 mm diameter (HPB 235) smooth steel bars were provided as compression reinforcement. Sufficient shear reinforcement was provided by ϕ 8 mm stirrups (HPB 235) spaced at 100 mm within the shear span and at 200 mm within the constant moment zone. The stirrups were wrapped with insulating tape at the stirrup-tension bar interfaces to prevent the stirrups from experiencing accelerated corrosion. As shown in Fig. 1, the corrosion specimens were corroded within 1,200 mm of the beam center.

The 28-day compressive strength of concrete was determined to be 36.7 MPa. The yield strengths of the tension reinforcement were 349 MPa and 318 MPa for the shear and compression reinforcement based on the results of a uni-axial tension test, respectively. Unidirectional CFRP flexible fabrics were used for strengthening and for U-shape anchoring using the wet lay-up procedure. The cured CFRP sheet had a design thickness of 0.111 mm, a tensile strength of 4114 MPa, an elastic modulus of 202 GPa, and an elongation at break of 2.33%, as provided by the manufacturer. The epoxy resin used for CFRP bonding is a formulation of a bisphenol-A-type epoxy resin and a hardener component that consists of blend sof polyamines; the resin and hardener components were mixed in a weight ratio of 2:1. The cured resin had a tensile strength of 41 MPa, an elastic modulus of 2.6 GPa and an elongation at break of 1.6%, as provided by the manufacturer.

Sustained Pre-loading Technique

As indicated in Fig. 2, the sustained pre-loading was applied using the bolted-anchorage system. The upper beam was for the combined load and corrosion pre-damage, and the lower beam was for the load pre-damage only. The unstrengthened specimen Ref was loaded first in a four-point bending configuration to determine its peak load, which was 41.2 kN with flexural failure. The load located at the one-third and two-third points of the beam span, and each took 25% of the peak load of specimen Ref, which is after the occurrence of flexural cracks and before yielding of the longitudinal bar. The beam self-weight (approximately 120 kg) was relatively small compared to the applied load (2010 kg); thus, its effect was ignored. The loading amplitude was controlled by the output of a digital torque wrench, which was calibrated by comparing the value of torque with the pull-out force indicated by a load cell. The sustained preloading was set to be 12 weeks. To compensate for the force loss due to creep and corrosion of the steel anchor, the anchor forces were re-calibrated every 15 days.

Accelerated Corrosion Technique before CFRP Strengthening

Before CFRP strengthening, accelerated corrosion along with the sustained loading technique were applied in the laboratory to induce corrosion in a reasonable period of time. Fig. 3 presents a schematic representation of the test setup for the accelerated corrosion. A sponge that absorbs NaCl solution was used to keep the concrete in the targeted corrosion areas wet. Stainless steel nets were attached to the sponge. The outside of the beam was then wrapped with a plastic sheet to keep the moisture in the sponge. The corrosion procedure can be divided into two phases, namely the electro-migration phase and the wetting–drying cycle phase. In the electro-migration phase, chloride ions were electro-migrated into the concrete cover using an electrochemical method. To simulate realistic chloride ingress in concrete, a NaCl solution with a concentration of 2 mol/L was first placed in the sponge to keep the concrete wet for more than 24 hrs. A stainless steel sheet was placed close to the neutral axis of the beam, as indicated in Fig. 1. The direction of the current flow was adjusted such that the outside stainless steel nets attached to the sponge became the cathode and the embedded stainless steel sheets served as the anode. Lastly, a constant voltage of 30 V was applied between the outside stainless steel nets and the embedded stainless steel sheets using a DC power source. Note that the use of the embedded stainless steel sheets as the anode is to achieve a relative non-uniform corrosion of the longitudinal steel bars, which reflects a more practical corrosion phase. The estimated time for the electro-migration phase was calculated to be 4.65 days based on Faraday’s law

Previous experience showed that cracks generate more rapidly in a dry environment than in a humid environment when an accelerated corrosion process is applied (Luping and Nilsson 1993). To simulate the degradation process that occurs in a real environment, a wetting–drying cycle process was used immediately after the electro-migration process. Each cycle of the wetting–drying process involved 3 days of drying followed by 4 days of wetting. The drying process was achieved by removing the plastic sheet to dry the sponge, whereas in the wetting process, the plastic sheet was reapplied to cover the beam and a 5% NaCl solution was placed in the sponge to wet the concrete. For the purpose of accelerated corrosion, a current density applied through the steel reinforcement (acting as the anode) and the stainless steel nets (acting as the cathode) of 0.15 mA/cm^2 was used in this study to avoid the damaging influence of high current on the steel and concrete interfacial bond (El Maaddawy and Soudki 2003). The estimated time for corrosion was calculated based on Faraday's law. In total, the wetting process was tested for 12 weeks.

CFRP Repair Scheme

After the reinforcing steel was corroded to the desired mass loss, the sustained load was released. The longitudinal and transverse cracks caused by steel corrosion or sustained loading, that appeared on the sides or the bottom face of the beams, were left untreated, with only the removal of surface dust for FRP bonding. The maximum crack width after pre-damage with sustained loading held was 0.20 mm and the CFRP was attached after the pre-loading was released. The residual crack width

was small so that no repairing effort was made. However in practice, the cracks of large width (>0.20 mm) should be repaired first before strengthening. The repair scheme consisted of flexural tension and U-wrap confinement sheets, as shown in Fig. 4. Two layers of flexural CFRP sheets with a width of 120 mm and a length of 1795 mm were bonded along the tension face of the beam with the fibers oriented parallel to the longitudinal direction of the beams. The CFRP U-wraps were 100 mm in width and 100 mm in height, and they were placed in an intermittent scheme along the shear span with a clear spacing of 50 mm.

Wetting-drying Cycles after CFRP Strengthening

A wetting–drying cycle process was induced two weeks after the CFRP strengthening. The sustained loading, which was 50% of the flexure strength of control specimen Ref, was applied first similar to the pre-damage process. The anchor forces were re-calibrated every 15 days. Each cycle of the wetting–drying process involved 12 hours of wetting by submerging the specimen into a 5% NaCl solution. The 12 hour drying process within one cycle was achieved by taking out the specimen to be dried with electric fans.

Test Setup and Instrumentation

All of the specimens were monotonically loaded to the peak load stage under four-point bending with a beam shear span to depth ratio of 3.0 at a loading step of 2kN/step before yielding of the tension reinforcement and 1.5 mm/step after yielding of the tension reinforcement. Three linear variable differential transformers (LVDTs) were used to measure the vertical displacements at the mid-span and at the loading point. The crack spacings and widths in the constant moment zone were recorded at the peak load stage.

Results and Discussion

Gravimetric Mass Loss Measurements

After loading the test specimens to failure, the tension steel bars were extracted and cleaned for the purpose of calculating mass loss following the ASTM G1-90 Standard (2002). Twelve coupons with a length of 100 mm within the targeted 1200 mm long corrosion area per steel bar per beam were used. The weight of the steel reinforcing bars without corrosion was determined by weighing the 100 mm long steel bars in the uncorroded zone of the same beam such that the weight of the extracted coupons after corrosion could be compared to the original weight and the mass loss due to corrosion could be estimated. The average measured values from 24 coupons per beam for the mass loss (corrosion degree) in the tension steel of the corroded beams are listed in Table 2. It can be concluded that the expected mass losses (10%) were achieved in the laboratory. The degree of

corrosion of the beams subjected to wetting-drying cycles after CFRP strengthening (L-C-40, L-C-80, L-C-120) differed less than that of the L-C-S beam without further exposure to wetting-drying cycles. The wetting-drying cycles after CFRP strengthening insignificantly affected the degree of corrosion.

Cracking behavior

For specimens Ref and L, the cracks developed conformably, and almost all major cracks expanded dramatically after yielding of the tension reinforcements. For specimen L-C, three of the six major cracks tended to open rapidly, whereas the remaining three cracks exhibited indistinctive changing after the tension reinforcements yielded. The strengthened beams exhibited a similar tendency, with specimens of the S series and L series showing consistent crack development and specimens of the L-C-S series showing inconsistent crack development. Fig. 5 shows the measured crack width distributions of the samples. This inconsistent crack development was attributed to the non-uniform corrosion of the tension reinforcements and hence the non-uniform bond between the tension reinforcements and concrete. The cracks that passed through more heavily corroded tension bars developed faster.

Fig. 6.a shows the crack pattern of two sides (front and back) and of the bottom for the beams after pre-damage with sustained loading or combined loading and corrosion. For specimens of the L series, flexural cracks primarily appeared within the constant moment zone. For specimens of the L-C series, in addition to the transverse cracks, two longitudinal corrosion cracks were observed at the side soffit of the beams, running parallel to the corroded steel reinforcing bars. Because the thickness of the side concrete cover (20 mm) is less than that of the bottom (25 mm), no corrosion cracks were observed in the bottom of the beam. Table 2 lists the average crack spacings and widths within the constant moment zone of specimens of the L series and L-S series. The average spacing of transverse cracks in the L-C series with the constant sustained load is 129 mm, which is close to that of the L series of 133 mm. The average crack width of the L-C series (0.19 mm) is larger than that of the L series (0.15 mm). The cracks were actually formed with the sustained loading before corrosion of the bar was initiated. However, corrosion of the bar weakened the bond between the bar and the concrete and resulted in a larger crack width, although the crack spacing is similar.

Table 2 also lists the average crack spacings and crack widths within the constant moment zone of loaded beams at the peak load stage, and the crack pattern is shown in Fig. 6.b. The specimens of the S, L-S, L-C-S series after strengthening have average crack spacings (width) of 74 (0.18) mm, 78(0.26) mm and 79 (0.21) mm compared to un-strengthened beams of 109 (1.01) mm, 115.0(0.94) mm and 131 (1.37) mm, respectively. The CFRP-strengthened beams had relatively smaller crack

246 spacings and widths than the un-strengthened beams. After CFRP strengthening, the effect of
247 pre-damage on the crack spacing and width is not as distinct as that in the un-strengthened cases.
248 The ability of CFRP to restrain crack development was verified. The sustained loading pre-damaged
249 beam exhibited an insignificant difference in crack spacing and width compared to beams without
250 pre-damage, indicating its negligible effect on the bar-concrete shear bonding properties.
251
252 The combined load and corrosion pre-damaged beam (L-C) had the largest crack width of 1.37
253 mm among the three un-strengthened beams. The accumulated corrosion products that cover
254 the surface of the bar may cause significant changes at the steel–concrete interface. Corrosion
255 products can alter the surface conditions at the boundary between the reinforcement and
256 concrete and hence influence the development of bond stresses. Additionally,
257 corrosion-induced cracking or spalling of the cover will reduce the confinement provided by
258 the concrete to the reinforcement, which is accompanied by a corresponding reduction in the
259 bond strength. Meanwhile, the reduction of the rib height of the deformed bars with increasing
260 levels of corrosion of the reinforcement weakens the interlocking forces between the ribs of the
261 bars and the surrounding concrete keys.
262
263 As shown in Table 2, the average crack spacings at the peak load stage of the strengthened
264 uncorroded beams subjected to further wetting- drying cycles are 67 mm, 75 mm and 70 mm

for specimens S-40, S-80 and S-120, respectively, which is less than a 10% difference from the value of 74 mm for specimen S without further exposure to wetting-drying. Similarly, the specimens L-C- S-40 and L-C-S-80 had average crack spacings of 76 mm and 75 mm at the peak load stage, respectively, which are approximately 4% smaller than the value of 79 mm for specimen L-C-S. On the other hand, the average crack spacing of specimen L-C-S-120 is 14% larger than that of specimen L-C-S. The wetting-drying cycles after strengthening exerted marginal effect on the degree of corrosion and the average crack spacing compared to the strengthened specimens without further exposure for both the corroded and un-corroded cases.

Analytical model

To better understand the cracking behavior of CFRP-strengthened beams, an analytical approach that considers the stresses of FRP-strengthened beam elements based on equilibrium and compatibility equations was developed. Fig. 7.a shows a longitudinal segment of a CFRP-strengthened beam between two adjacent cracks subjected to uniaxial tensile force. The length of this segment, S_c, represents the crack spacing. The free body diagram of the substrate and CFRP laminate with a length of dx is shown in Fig. 7.b. The equilibrium of forces acting on the concrete and CFRP segment can be written as follows:

$$\frac{dF}{dx} = \frac{d\sigma_c(x)}{dx} A_{ct} = -\left(\sum O_r \tau_{bc}(x) + \sum O_{CFRP} \tau_{bCFRP}(x)\right) \quad (1)$$

where $\tau_{bc}(x)$ and $\tau_{bCFRP}(x)$ denote the bond stress at the reinforcement-concrete interface and at the reinforcement-CFRP interface at the stabilized crack stage, which is assumed to follow a parabolic variation, as shown in Fig. 7.c. The peak bond stress τ_{bcm} or τ_{bCFRP} occurs at the midsection between the two zero points. This bond stress distribution closely agrees with the experimental observations of Jiang et al. (1984) and Kankam (1997) for uncorroded bars and of Zhao et al. (2013) for corroded bars. O_r and O_{CFRP} denote the perimeter of the tension reinforcement in concrete and CFRP, respectively, and A_{ct} denotes the effective tension area of concrete and can be determined according to Zhang et al (2011).

For a given element between two adjacent cracks, the expected location for the maximum concrete tensile stress is at the midway point (zero-slip point). At the stabilized crack stage, the tensile stress of concrete at the zero-slip point (σ_{cs}) cannot be greater than the tensile strength (f_{ct}), regardless of the load increase. This condition corresponds to the stabilized crack spacing S_{cs} for the case in which the maximum concrete tensile stress $\sigma_{cmax} \leq f_{ct}$. Therefore, based on Eq. 1, the following equations can be derived following the shear stress distributions in Fig. 7.c:

301 $$\sigma_{cs} = \int_{S/2}^{0} -\frac{\left(\sum O_r \tau_{bc}(x) + \sum O_{CFRP} \tau_{bCFRP}(x)\right)}{A_{ct}} dx = \frac{\left(\sum O_r \cdot \frac{4}{3} \cdot \frac{1}{2} \cdot \frac{S}{2} \cdot \tau_{bcm} + \sum O_{CFRP} \cdot \frac{4}{3} \cdot \frac{1}{2} \cdot \frac{S}{2} \cdot \tau_{bCFRPm}\right)}{A_{ct}}$$
$$= \frac{S\left(\sum O_r \tau_{bcm} + \sum O_{CFRP} \tau_{bCFRPm}\right)}{3A_{ct}} \leq f_{ct}$$

302 (2)

303

304 The stabilized crack spacing of the substrate concrete layer is then expressed in the following way:

305

306 $$S_{cs} = \frac{3 f_{ct} A_{ct}}{\left(\sum O_r \tau_{bcm} + \sum O_{CFRP} \tau_{bCFRP}\right)} \quad (3)$$

307

308 The bond strength between the reinforcement (steel bar and CFRP laminate) and concrete depends
309 primarily on the compressive strength, the cover thickness of concrete, the confinement condition,
310 and the surface condition of the reinforcement. The peak bond stress without corrosion damage (τ_{bcm})
311 can be calculated using the fib Model Code equation (2010).

312

313 The bond strength at the interface between a steel bar and concrete is affected by the corrosion of
314 the steel bar. Transverse reinforcement can control the development of cracking induced by steel
315 corrosion and therefore restrain the bond degradation. Numerous studies have focused on the effect
316 of corrosion on the bond between steel bars and concrete. In this study, the bond strength with bar
317 corrosion (τ_{bcmc}) is represented by the following equation according to the experimental data from

318 Zhao et al (2013):

319

320 $$\tau_{bcmc} = k_p \, \tau_{bcm} \quad (4)$$

321

322 where k_p is a coefficient that reflects the corrosion effect and can be calculated in the following

323 way:

324 without transverse reinforcement

325 $$k_p = \begin{cases} 1 - 2.79\eta_{average} & \eta_{average} < 4\% \\ 1.58 - 17.21(\eta_{average} - 0.08) & 4\% \le \eta_{average} < 8\% \\ 0.20 & \eta_{average} \ge 8\% \end{cases} \quad (5a)$$

326 with transverse reinforcement

327 $$k_p = \begin{cases} 1 & \eta_{average} < 5.5\% \\ 1 - 15.00\,(\eta_{average} - 0.055) & 5.5\% \le \eta_{average} < 9.5\% \\ 0.40 & \eta_{average} \ge 9.5\% \end{cases} \quad (5b)$$

328

329 where $\eta_{average}$ denotes the average degree of bar corrosion, which is the same as the mass loss.

330 Fig. 8 shows the comparison between the test data and the bond strength from the above equation.

331 τ_{bcmc} can substitute τ_{bcm} in Eq. 3 in the case of bar corrosion. The increment of bar-concrete bond

332 strength at a low degree of corrosion was not considered in the proposed equation. The test data

333 with bar corrosion degree less than 3% in the cases without stirrup and 5% in the cases with stirrup

334 were not used for the best fitting process. Because the wetting-drying cycles up to 120 cycles after

CFRP strengthening did not affect the crack spacing in the strengthened beams, the reduction in the CFRP-concrete bond strength τ_{bCFRP} was not considered in the current model.

Considering the effect of the strain gradient, the average crack spacing in the CFRP-strengthened beam under flexure load can be predicted as follows:

$$S_{sf} = k_1 S_{cs} \quad (5)$$

where k_1 is the coefficient to account for the strain gradient = $(\varepsilon_1 + \varepsilon_2)/2\varepsilon_1$ according to *CSA S474* (2004), and ε_1 and ε_2 are the largest and smallest tensile strains in the effective tension zone.

Verification

The measured average crack spacing is used to verify the applicability of the proposed analytical model. Due to the existence of transverse reinforcements, Eq. 4-2 was used to calculate the maximum bond shear stress of both substrate concrete layers for various corrosion degrees. The calculation results for CFRP-strengthened beams with or without pre- or post-damage are shown in Table 2 and Fig. 9. For specimen L-C, the calculated crack spacing is considerably larger than that

of the test result. The sustained loading (50% of the peak load of the control beam Ref) induced concrete cracks before bar corrosion; therefore, the crack spacing cannot be increased, even with further bar corrosion. It is expected that if the bar corrosion occurs before any loading damage, the tested crack spacing is closer to that predicted by the proposed model. The mean ratio of the calculated $S_{sf.}$ and experimental S_{exp} for the rest of the specimens is 0.97, with a standard deviation of 0.09. The analytical values agreed with the experimental values, which verifies the accuracy of the proposed model, indicating that the proposed prediction method is applicable.

It should be noted that 1) the proposed model assumes the monolithic responding of CFRP laminate and substrate concrete, and therefore, it is not applicable for the case in which debonding between the substrate and CFRP occurs before the stabilized cracking stage is reached; 2) the effect of concrete cracks caused by pre-damage on the cracking spacing of strengthened beams was not considered in the proposed model; and 3) the proposed model is verified for the CFRP-strengthened beams with no damage, pre-damage with sustained loading and pre-damage with combined loading and bar corrosion. The applicability of the model for the beams in which bar corrosion is initiated after CFRP strengthening should be confirmed with further experimental proofs.

Conclusions

This study investigated the effects of three types of pre- and post-damages on the cracking behaviors of CFRP-strengthened RC beams. The non-uniform corrosion of tension reinforcements

in the concrete substrate led to inconsistent crack development in RC beams, and cracks that passed through more heavily corroded tension bars developed faster. Without CFRP strengthening, the combined load and corrosion pre-damaged beam had the largest crack spacing and width. After CFRP strengthening, the effects of pre- or post-damage on the crack spacing and width are not as distinct as in the un-strengthened cases. The sustained loading pre-damaged beam exhibited an insignificant difference in crack spacing and width compared to beams without pre-damage, indicating its negligible effect on the bar-concrete bond properties. The wetting-drying cycles after strengthening exhibited marginal effects on the average crack spacing and width compared to the strengthened specimens without further damage for both the corroded and un-corroded cases.

A crack spacing model was then developed by considering the equilibrium and compatibility equations of the CFRP-strengthened beam element. The new model can account for the influence of major parameters, such as the quantities and total perimeters of reinforcement across the crack, the tensile strength of the concrete substrate, and the characteristics of the bond between the concrete and reinforcement in the substrate with or without bar corrosion. To validate the proposed model, the values of the average crack spacing predicted using the proposed model were compared with experimental results. The proposed model performs well with respect to the experimentally measured response.

Acknowledgments

The financial support from the Zhejiang Provincial Natural Science Foundation of China（Grant No. LR12E08001）and the Natural Science Foundation of China (Grant Nos. 81308494) is greatly appreciated.

References.

ASTM. Standard G1-90 (2002). Practice for preparing, cleaning, and evaluating corrosion test specimens, West Conshohocken, PA.

Badawi M. and Soudki K., (2010). “CFRP Repair of RC Beams with Shear-Span and Full-Span Corrosions”, J. Compos.Constr., 14, pp.323-335.

Bonacci, J. F., and Maalej, M., (2000). “Externally bonded fibrereinforced polymer for rehabilitation of corrosion damaged concrete beams.” ACI Struct. J., 97(5), pp.703–711.

Canadian Standard Associations (2004). S474 concrete structures. Mississauga (Ontario, Canada): Canadian Standard Associations.

Ceroni, F., and Pecce, M., (2009). “Design provisions for crack spacing and width in RC elements externally bonded with FRP”, Composites Part B: Engineering, 40(1), pp.17-28.

Debaiky, A. S., Green, M. F., and Hope, B. B., (2002). “Carbon fiber reinforced polymer wraps for corrosion control and rehabilitation of reinforced concrete columns.” ACI Mater. J., 99(2), pp.129–137.

El Maaddawy, T., and Soudki, K. (2003). “Effectiveness of impressed current technique to simulate corrosion of steel reinforcement in concrete.”, J. Mater. Civ. Eng., 15(1), pp. 41–47.

El Maaddawy, T., and Soudki, K., (2005) “Carbon-fiber-reinforced polymer repair to extend service life of corroded reinforced concrete beams.” J. Compos. Constr., 9(2), pp.187–194.

Fib model code (2010), first complete draft, bulletin 55/1, International Federation for Structural Concrete.

Jiang, D., Shah, S. P, and Andonian, A. (1984). “Study of the Transfer of Tensile Forces by Bond, ACI Structural Journal, 81(3), pp. 251-259.

Holloway LC, Leeming MB, (1999). Strengthening of reinforcedconcrete structures. UK: Woodhead Publishing Limited.

Kankam, C. (1997). “Relationship of Bond Stress, Steel Stress, and Slip in Reinforced Concrete,” Journal of Structural Engineering, ASCE, 123(1), pp. 79-85.

Lau D, Büyüköztürk O., (2010). “Fracture characterization of concrete/epoxy interface affected by moisture.” Mechanics of Materials, 42(12), pp. 1031-42.

Luping T., Nilsson L.O. (1993), “Rapid determination of the chloride diffusivity in concrete by applying an electric field”, ACI Mater. J. 89, pp.49–53.

Masoud, S., Soudki, K., and Topper, T., (2001). “CFRP-strengthened and corroded RC beams under monotonic and fatigue loads.” J. Compos. Constr., 5(4), pp. 228–236.

428 Masoud S. and Soudki K., (2006). “Evaluation of corrosion activity in FRP repaired RC beams”,
429 Cement & Concrete Composites, 28, pp. 969–977.
430 Nossoni, G., and Harichandran, R., (2009). “Improved repair of concrete structures using polymer
431 concrete patch and FRP overlay.” J. Mater. Civ. Eng., 22(4), pp.314–322.
432 Oehlers D.J. (2001). “Development of design rules for retrofitting by adhesivebonding or bolting
433 either FRP or steel plates to RC beams or slabs inbridges and buildings”, Composites Part A
434 2001;32:1345–55.
435 Raoof, M., Hassanen, MAH., (2000). “Peeling failure of reinforced concrete beams with
436 fibre-reinforced plastic or steel plates glued to their soffits”. Proceedings of the Institution of
437 Civil Engineers, Structures and Buildings, 140, pp. 291–305.
438 Tuakta C, Büyüköztürk O., (2011). “Deterioration of FRP/concrete bond system under variable
439 moisture conditions quantified by fracture mechanics”. Composites Part B: Engineering. 42(2),
440 pp. 145-54.
441 Wang C.Y., Shih C.C., Hong S.C. and Hwang W.C., (2004). “Rehabilitation of Cracked and
442 Corroded Reinforced Concrete Beams with Fiber-Reinforced Plastic Patches” J. Compos.
443 Constr.8, pp.219-228.
444 Wang, C.Y., Ling, F.S., (1998). “Prediction model for the debonding failure of cracked RC beams
445 with externally bonded FRP sheets”. Proceedings of the Second International Conference of
446 Composites in Infrastructure (ICCI), Arizona, USA, pp.548–562.

Wootton, I. A., Spainhour, L. K., and Yazdani, P. E., (2003). “Corrosion of steel reinforcement in carbon fiber-reinforced polymer wrapped concrete cylinders.” J. Compos. Constr., 7(4), pp.339–347.

Zhang, D.W., Ueda, T., and Furuuchi, H., (2011). “Average Crack Spacing of Overlay-Strengthened RC Beams”. Journal of Materials in Civil Engineering, ASCE, 23(10), pp.1460-1472.

Zhang, D.W., Ueda, T., and Furuuchi, H., (2012). “A Design Proposal for Concrete Cover Separation in Beams Strengthened by Various Externally Bonded Tension Reinforcements”, Journal of Advanced Concrete Technology, JCI, 10(9), pp. 285-300.

Zhao Y.X., Lin H.W., Wu, K., Jin, W.L., (2013). “Bond behavior of normal/recycled concrete and corroded steel bars”, Construction and Building Materials, 48, pp.348-359.

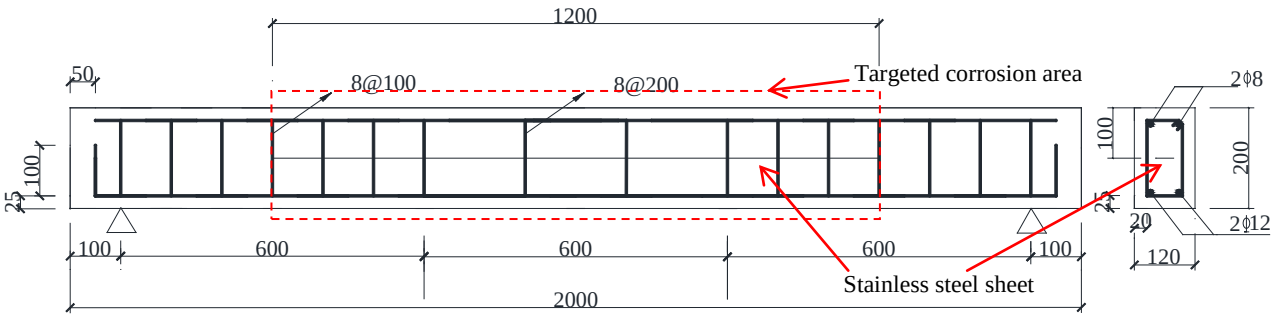

Fig. 1 Geometry and reinforcement information of test specimens (unit: mm)

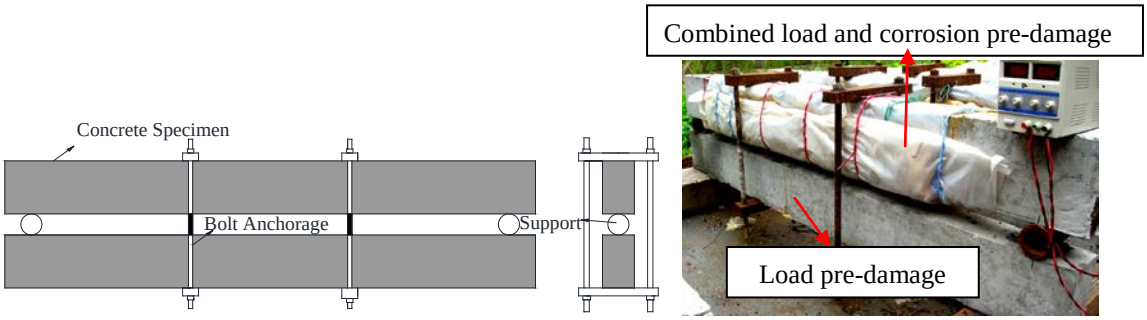

Fig. 2 Apparatus for sustained loading pre-damage

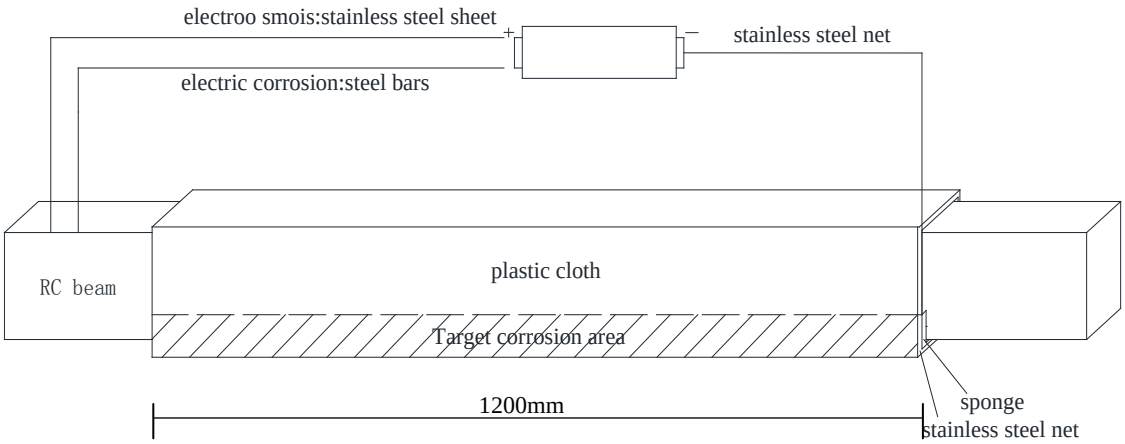

Fig. 3 Accelerated corrosion techniques (unit: mm)

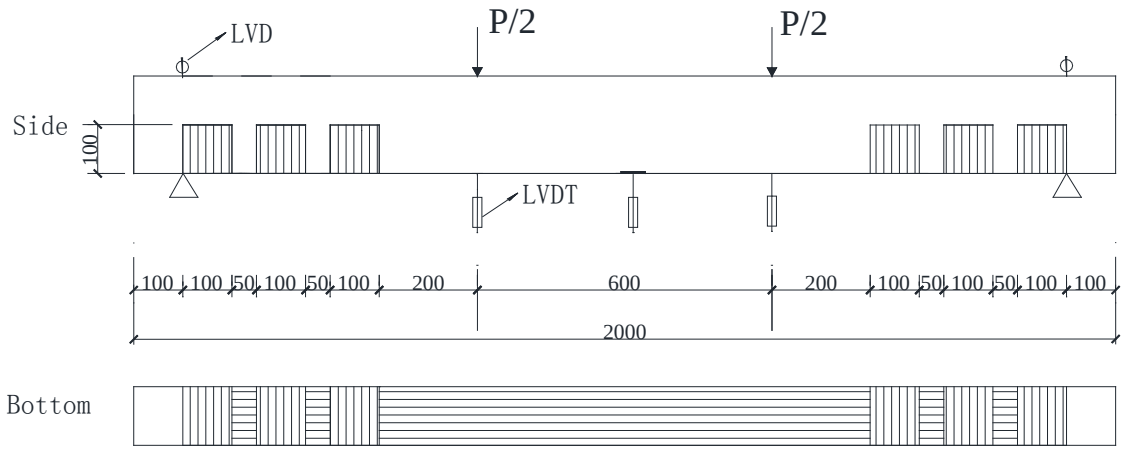

Fig. 4 CFRP strengthening and arrangement of strain gauges (unit: mm)

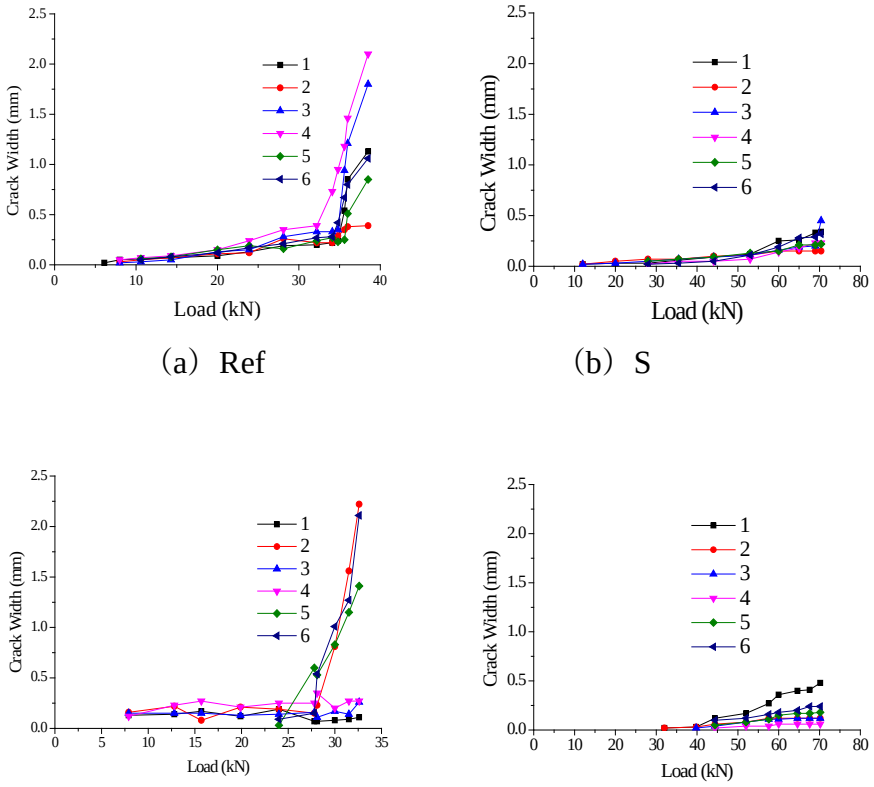

Figure 5 Sample crack width distribution of tested specimens
(Six major cracks from all the flexural cracks within the constant moment zone)

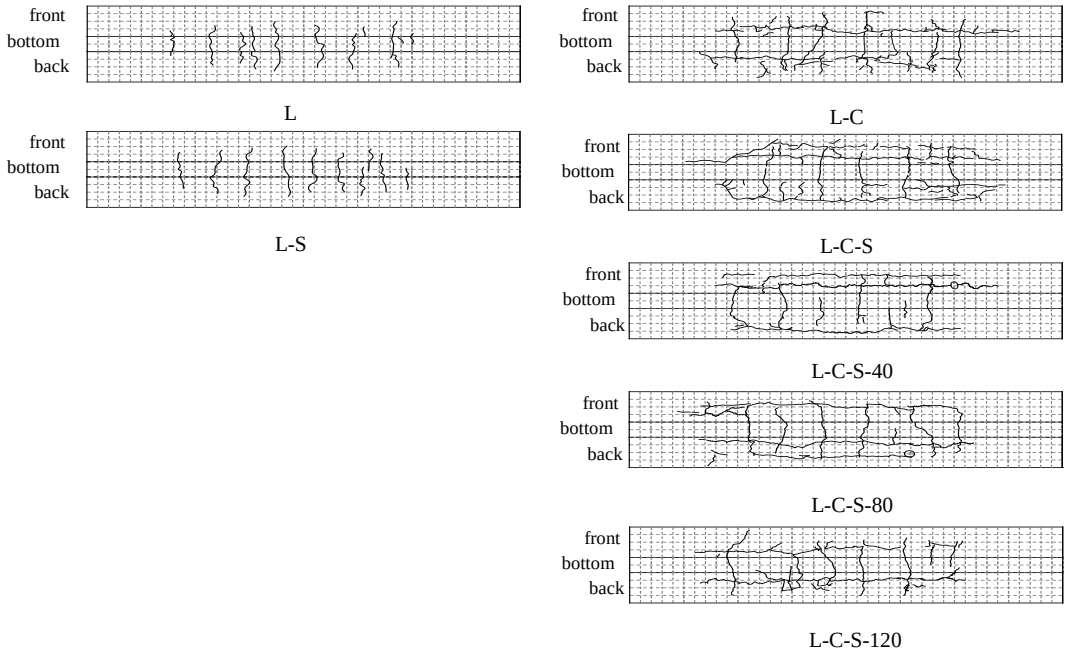

a. After pre-damage (destabilized crack)

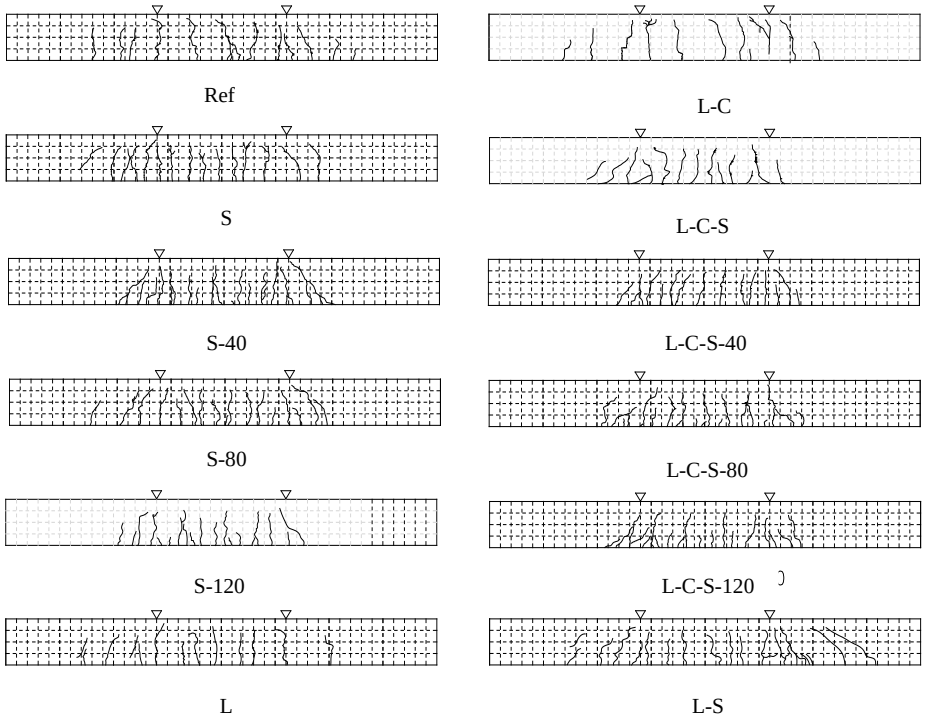

b. Peak load stage (stabilized crack, front face)

Fig. 6 Crack pattern of test specimens

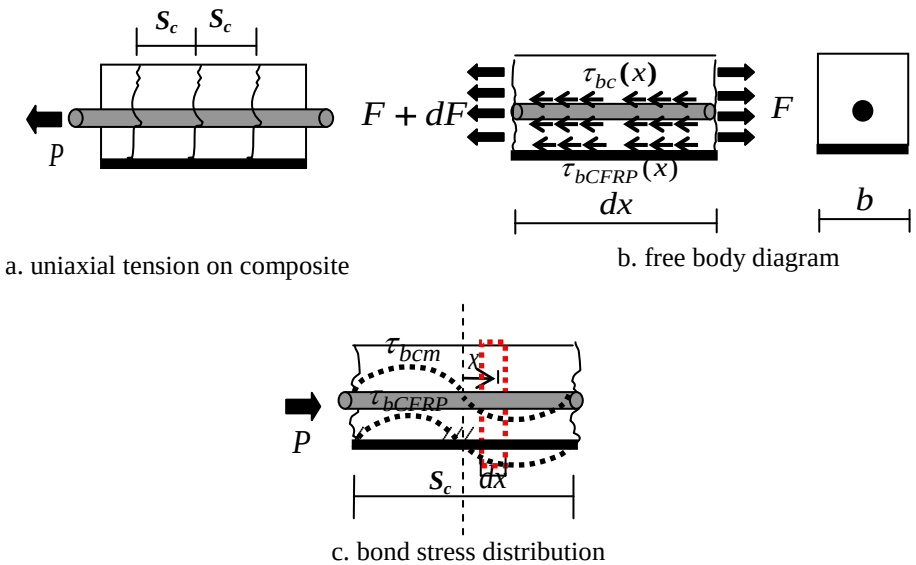

a. uniaxial tension on composite

b. free body diagram

c. bond stress distribution

Fig. 7 Element analysis of composite

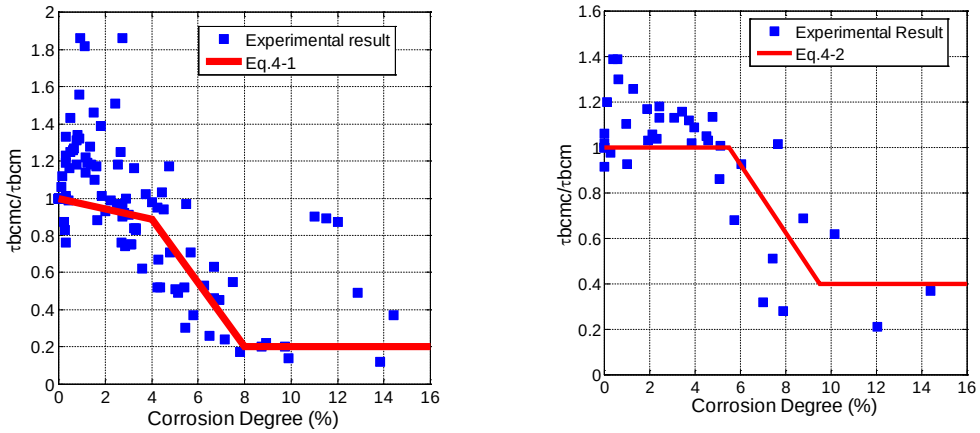

a. without stirrup

b. with stirrup

Fig. 8 Effect of bar corrosion on bar-concrete bond strength
(Experimental database is from Zhao et al (2013))

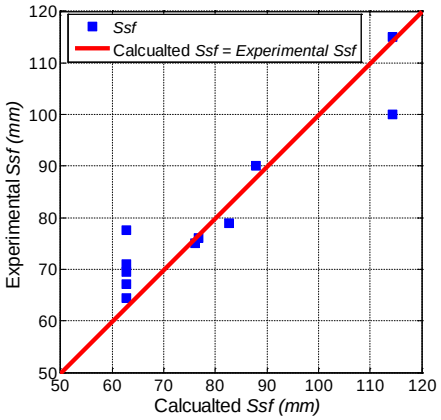

Fig. 9 Comparison between calculated and experimental crack spacing

Table 1 Parameters of test specimens

Series	Specimen	Pre-damage		Number of CFRP layers	U-shape anchorage
		Loading ratio*	Corrosion degree		
	Ref	—	—	—	—
S series	S	—	—	2	○
	S-40	—	—	2	○
	S-80	—	—	2	○
	S-120	—	—	2	○
L series	L	50%	—	—	—
	L -S	50%	—	2	○
L-C series	L-C	50%	10%	—	—
	L-C-S	50%	10%	2	○
	L-C-S-40	50%	10%	2	○
	L-C-S-80	50%	10%	2	○
	L-C-S-120	50%	10%	2	○

*Loading ratio= value of sustained load/expected peak load of specimen Ref-B

Table 2 Crack spacing and width of test specimens

Series	Specimen	Average corrosion degree	Average crack spacing			Average crack width	
			After Pre-damage	Peak load stage*		After Pre-damage	Peak load stage
				Tested	Calculated		
		%			mm		
	Ref-B	0	-	109	114	-	1.01
S series	S	0	-	74	63	-	0.18
	S-40	0	-	67	63	-	0.20
	S-80	0	-	75	63	-	0.19
	S-120	0	-	70	63	-	0.17
L series	L	0	131	115	114	0.15	0.94
	L -S	0	134	78	63	0.15	0.26
L-C series	L-C	10.6	131	131	271	0.18	1.37
	L-C-S	9.4	121	79	83	0.17	0.21
	L-C-S-40	8.6	138	76	77	0.18	0.21
	L-C-S-80	8.5	126	76	76	0.20	0.24
	L-C-S-120	10.0	129	90	88	0.20	0.18

* Only the cracks with lengths greater than 50 mm were counted for cracking spacings and widths at the peak load stage.